

Research on the comprehensive performance of PrFeB magnets for synchrotron radiation and free electron laser

Yong-Zhou He¹ · Xiao-Qing Bao² · Wei Zhang¹ · Qiao-Gen Zhou¹

Received: 3 November 2018 / Revised: 5 March 2019 / Accepted: 3 April 2019 / Published online: 11 July 2019

© China Science Publishing & Media Ltd. (Science Press), Shanghai Institute of Applied Physics, the Chinese Academy of Sciences, Chinese Nuclear Society and Springer Nature Singapore Pte Ltd. 2019

Abstract PrFeB magnets, which possess excellent magnetic properties at low temperatures, have important application value as cryogenic permanent magnet undulators for synchrotron radiation sources and free electron lasers. In this research study, several high-performance PrFeB magnets (P42H, P48SH, and P48UH) were prepared, and their performance was comprehensively examined, including evaluations of their magnetic properties, microstructures, uniformity, and stability. Next, their application prospects were analyzed and discussed. In China, the first cryogenic permanent magnet undulators (CPMUs) with P48SH magnets with 18 mm cycle lengths have been developed. When the temperature is 80 K and the gap is 6.0 mm, the magnetic field measurement results of the CPMU showed that the effective magnetic field peak was approximately 0.92 T, yielding an increase of 11.76% relative to operation at 300 K, with an RMS phase error of about 4.99°.

Keywords PrFeB magnets · Cryogenic permanent magnet undulators · Grain boundary diffusion method · Free electron laser

This work was supported by project of the State Key Lab of Advanced Metals and Materials (No. 2016-Z03).

✉ Yong-Zhou He
heyongzhou@sinap.ac.cn

¹ The Shanghai Institute of Applied Physics, Chinese Academy of Sciences, Shanghai 201800, China

² The University of Science and Technology Beijing (USTB), Beijing 100083, China

1 Introduction

Permanent magnet undulators are typical Halbach magnetic structures [1]. They have become one of the key pieces of equipment used in high-energy physics and are commonly used in synchrotron radiation facilities and free electron laser devices [2, 3]. NdFeB magnets [4], which were discovered in 1983, have been widely applied, and are currently one of the key permanent magnets used for undulators [5]. PrFeB and NdFeB have similar crystal structures, and their theoretical remanence B_r and intrinsic coercivity H_{cj} are very similar at about 25 °C. The aforementioned PrFeB magnets are characterized by a lack of spin reorientation effects (SRT) [6], which results in excellent magnetic properties at low temperatures; they have therefore been found to be more suitable as magnetic sources for cryogenic permanent magnet undulators (CPMUs) [7–9]. However, if PrFeB magnets are to be used in synchrotron radiation and free electron laser applications, the following problems must be resolved:

- (1) With higher comprehensive magnetic properties, the higher B_r at low temperature can potentially result in the CPMU having a higher magnetic field peak value. Furthermore, the higher H_{cj} at room temperature can potentially cause certain anti-demagnetization effects, which can affect the properties of the CPMU. Owing to the temperature coefficient and other factors, differences in the magnetic properties at room temperature and at low temperatures have often been observed.
- (2) With their excellent magnetic field homogeneity, the magnetic deflection angle of a PrFeB magnet with a small length-to-diameter ratio for a typical CPMU is

approximately less than 1° . In addition, the consistency of the total magnetic moment, M_r , has been observed to be less than 2%. Moreover, the magnetic field uniformity is known to be closely related to the preparation methods and composition design.

- (3) With their favorable magnetic field stability, CPMUs with hundreds of magnets with Halbach magnetic circuit loads are characterized by large demagnetization fields when installed at room temperature. However, the H_{cj} values of PrFeB magnets will exhibit a significant decline when they undergo higher-temperature baking. Therefore, the PrFeB magnets are required to exhibit no obvious irreversible demagnetization in higher-temperature environments.

In this paper, three types of PrFeB magnets were designed and prepared. Their performance was analyzed comprehensively by studying and analyzing several features, such as their magnetic properties, microstructures, magnetic field uniformity, and magnetic field stability. On this basis, the first cryogenic permanent magnet undulator (CPMU18) with P48SH magnets was developed in China.

2 Preparation of the PrFeB

As part of the preparation of the P42H and P48SH CPMUs, appropriate adjustments were made for the NdFeB magnets. The P48SH magnets were used as substrates for the P48UH magnets, which had been developed using a grain boundary diffusion (GBD) method [10–12]. The main purpose of preparing the P42H magnets was to understand the performance characteristics of the pure PrFeB magnets. Therefore, the following processes were completed: ① By using pure Pr, the mechanism by which the magnetic properties of the nearly pure PrFeB magnet changed at low temperatures was examined. ② With no heavy rare earth elements, Dy and Tb were used to improve the absolute value of the temperature coefficient. ③ For the purpose of increasing the H_{cj} , trace elements M (such as Cu, Al, and Nb) were added. The main purpose of preparing the P48SH magnets was to further improve the comprehensive performance. Therefore, this study completed the following processes: ① The Fe content was raised to improve the Br, and the Pr content was reduced to the theoretical value of 31.0%. ② Trace elements M (such as Ca, Zr, and Cr) were added to further enhance the H_{cj} . In addition, in order to create a “residual magnetization M_r platform” at 50 K, 10% Nd was added to replace part of the Pr. The main purpose of preparing the P48UH magnets was to improve the H_{cj} of the P48SH through a GBD method, which could potentially greatly improve the

stability of the magnetic field. Therefore, the following were determined in this study: ① As a diffusion powder, TbF_3 can partially react with the main phase of $Pr_2Fe_{14}B$ to form $(Pr,Tb)_2Fe_{14}B$ within the higher anisotropic field H_A . ② The effects of the GBD process are closely related to the orientation thicknesses of the magnets. Therefore, block P48SH magnets with a thinner orientation thickness were used as the substrate. The components along with some of the parameters of the three types of magnets used in this study are listed in Table 1.

3 The performance of PrFeB magnets

3.1 Magnetic properties

Figure 1a shows the demagnetization curves of the three PrFeB magnets at room temperature [13]. As can be seen in the figure, for the P42H, P48SH, and P48UH magnets, the Br values were 1.30 T, 1.38 T, and 1.37 T, respectively. The H_{cj} values were 1580 kA/m, 2080 kA/m, and 1400 kA/m, respectively. The $(BH)_{max} + H_{cj}$ values were 58.8, 65.9, and 74.7 [11], respectively. The $(BH)_{max} + H_k$ values (which are more meaningful in the design of magnetic circuits) were 57.4, 65.3, and 66.1, respectively, and the H_k/H_{cj} ratios were 0.92, 0.97, and 0.77, respectively. Following the optimization of the composition and preparation method, it was found that the Br, H_{cj} , and H_k/H_{cj} values of the P48SH magnet were improved when compared with the P42H magnet. Furthermore, when compared with P48SH, the Br of the P48UH displayed no significant changes. The H_{cj} had increased by approximately 560 kA/m, and the square degree (H_k/H_{cj}) had deteriorated. These results were determined to have been caused by the non-uniform diffusion of the TbF_3 in the magnet, which was the

Table 1 Components and part process parameters of the PrFeB magnets

Grade	Component (%)				
	Pr	Nd	B	Fe	M
P42H	31.80	0.00	1.03	66.00	1.15
P48SH	28.08	3.12	1.00	66.60	1.50
P48UH	The base material is P48SH, and the GBD powder is TbF_3				
Grade	Partial process parameters				
	Powder size (μm)	Magnetic field intensity (T)	Heat treatment temperature ($^\circ\text{C}$)	Density (g/cm^3)	
P42H	2–15	1.80	1050–890–465	7.44	
P48SH	2–10	2.02	1060–890–430	7.51	
P48UH			890 + 465	7.56	

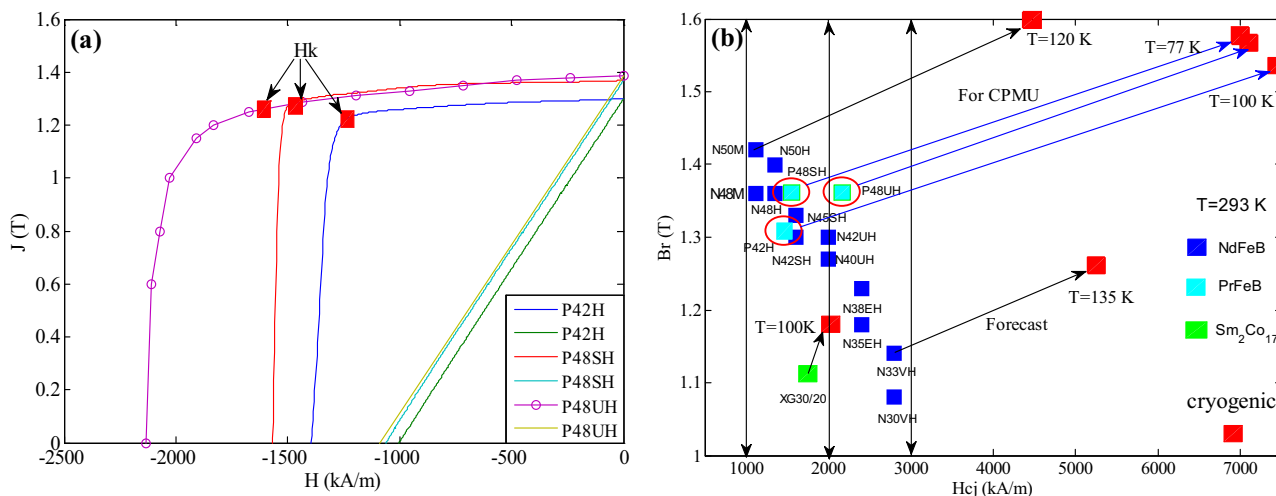


Fig. 1 (Color online) Magnetic properties of PrFeB: **a** room temperature demagnetization curve and **b** magnetic properties at low temperature

result of the demagnetization inconsistency. Figure 1b details the typical cryogenic magnetic properties of rare earth magnets. It can be seen in the figure that, at low temperatures, the Br and Hcj of an SmCo magnet [such as the XG30/20(CHC)] were not very high. In addition, the Br and Hcj of NdFeB magnets (such as the N33VH and N50 M) increased. However, the SRT only showed a relatively limited increase in the Br. The Br and Hcj of the PrFeB magnets with no SRT were observed to be greatly improved. When compared with the values at 293 K, at 77 K, the Br values of the P42H, P48SH and P48UH were determined to have increased by 15.4%, 13.9%, and 13.5%, respectively, and the Hcj had increased by almost more than three times. It was found that, between 293 and 77 K, the average absolute temperature coefficient values of the Hcj and Br of the three types of magnets had gradually decreased. Between 293 and 77 K, the Br of the SmCo (XG30/20) and the NdFeB (N33VH) magnets were determined to have increased by 6.0% and 8.0%, respectively. These findings were closely related to the composition design of the permanent magnet.

3.2 Microstructure

Figure 2 details the XRD patterns of the P42H, P48SH, and P48UH magnets. As can be seen in the figure, the ratios of the (006) peak to the (105) peak for P42H, P48SH, and P48U were 1.02, 1.16, and 1.31, respectively. Furthermore, when compared with P42H, the orientation degree of P48SH was observed to have been improved (for example, the 006/105 ratio [4] increased) [13]. These findings were determined to be closely related to the increased orientation of the magnetic field and the optimization of the powder particle size distribution. When compared to P48SH, the orientation degree of P48UH

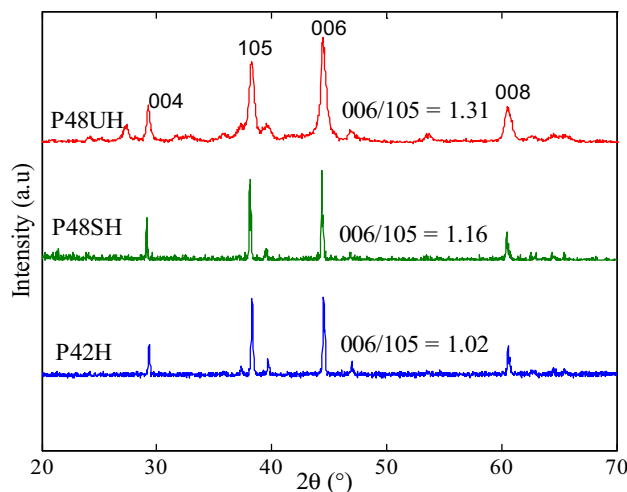


Fig. 2 (Color online) XRD diffraction patterns of PrFeB

displayed further improvements (for example, the 006/105 ratio increased again). This indicated that there was a major difference in the diffusion concentration of TbF₃ along the different crystal faces of the main phase of the Pr₂Fe₁₄B. Furthermore, along the parallel orientation plane (006), the diffusion effects were observed to be stronger than along plane (105), which forms a 15.44° angle with the (006) plane.

Figure 3 displays backscattering images of the P42H, P48SH, and P48UH magnets. The dark gray region represents the base magnetic phase (Pr,Tb)₂Fe₁₄B, and the bright white or grayish white region denotes the Pr-/Tb-rich phase. It can be seen in the figure that the intergranular Pr-/Tb-rich phase of the P42H magnet was relatively concentrated, and the number of grain boundary cracks was greater. For the P48SH magnets, there was a relatively uniform and very thin Pr-/Tb-rich phase distributed

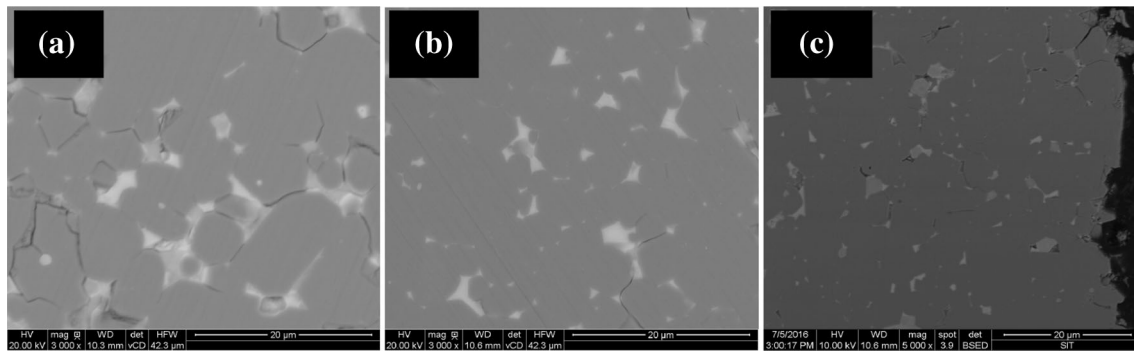


Fig. 3 SEM images: **a** P42H, **b** P48SH, and **c** P48UH

between the grain boundaries. When compared with the P48SH magnets, the grain boundaries of the P48UH magnet showed a more uniform distribution of the Pr-/Tb-rich phase, which formed an approximate grid with the Pr-/Tb-rich phase between the grain boundaries. The grayish white area was increased after the GBD process, which indicated that in the main magnetic phases $(\text{Pr,Tb})_2\text{Fe}_{14}\text{B}$ [12], the Pr near the boundaries was replaced by Tb.

Figure 4 details the relative concentrations of Pr and Tb along the orientation direction (from the surface to the interior) of the P48UH magnet as determined by electron probe micro-analysis (EPMA). As shown in Fig. 4a, on the surface of the magnet in the 0–17 μm range, the relative Pr concentration changed rapidly. For example, the Pr content decreased sharply closer to the surface of the magnet, which was caused by the Pr of the magnet's surface having undergone major losses during the GBD process. Within the 17–105 μm range, the relative concentration of Pr was observed to decrease following the grain boundary diffusion, and the closer to the surface of the magnet, the greater the decrease. These findings indicated that the closer to the surface, the more Pr was replaced by Tb. Figure 4b shows that the relative concentration of Tb increased significantly

following the grain boundary diffusion process, and the closer to the surface of the magnet, the more the Tb increased. These findings also indicated that the GBD effect was closely related to the orientation thicknesses of the magnets. For example, smaller thicknesses produced more obvious effects. The GBD process can potentially greatly improve the H_{cJ} of a magnet. However, the technical characteristic constraints tend to result in different positions, and the increased amplitudes of the H_{cJ} have been found to not be uniform. Figure 1a shows that the demagnetization curve of the P48UH had an average value, and it could not display the H_{cJ} value at each point.

3.3 Magnetic uniformity

Figure 5 details the total moment M_r consistency, along with the magnetization angle of the PrFeB (sample size: 50 mm \times 30 mm \times 6.6 mm; orientation: 6.6 mm) [14]. As shown in Fig. 5a, the differences in the M_r between the three types of magnets were not particularly large, and the M_r value fluctuated within a range of approximately 0.8%. However, the micro-fluctuation displayed obvious differences during the testing of the fifteen samples. For

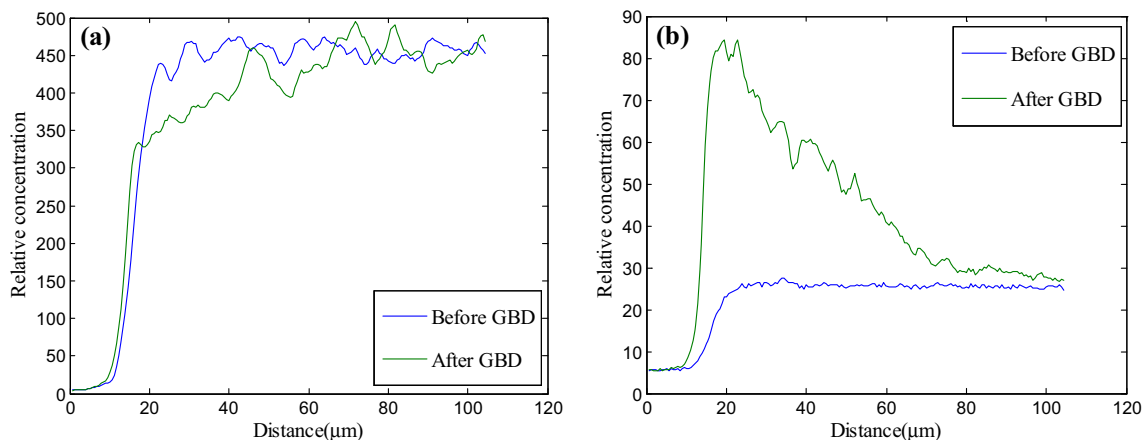


Fig. 4 (Color online) Election probe micro-analyzer (EPMA) relative concentration of P48UH: **a** Pr and **b** Tb

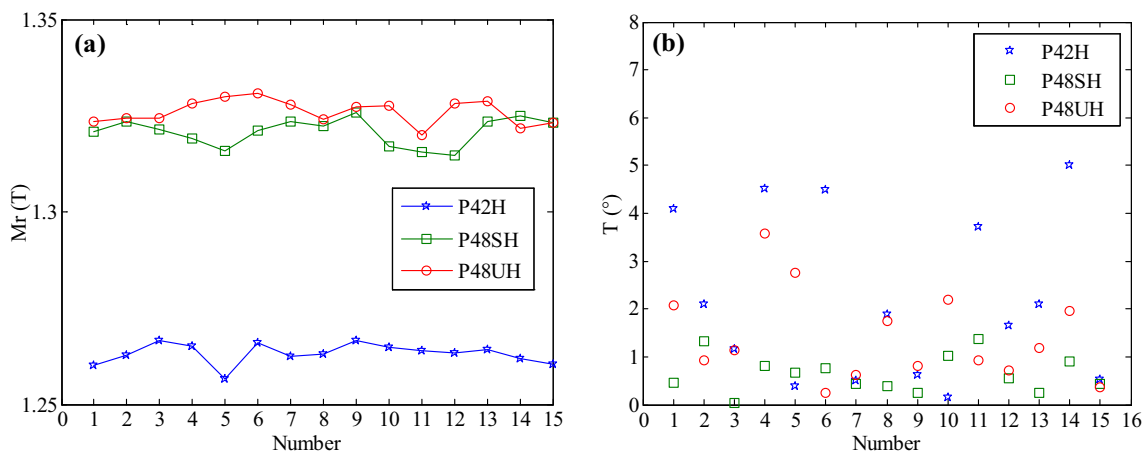


Fig. 5 (Color online) Field homogeneity of the PrFeB magnet: **a** moment consistency and **b** magnetization angle

example, in regard to the P42H magnets in exon 5, the other magnets' fluctuation ranges were only approximately 0.5%. For the P48SH magnets in exon 5, 11, 14, and 15, the M_r consistencies of the other magnets were less than 0.4%. There were obvious microscopic fluctuations observed for the P48UH magnets. As detailed in Fig. 5b, the magnetic angles of the three types of magnets displayed major differences. The ratio of the P42H, P48SH, and P48UH magnets with less than 1° was approximately 26.7%, 80%, and 46.7%, respectively. Therefore, after optimizing the composition designs and processes, the P48SH magnets exhibited a substantial improvement in orientation degree which gave them a small magnetization angle relative to the P42H magnets. In regard to the P48UH magnets with GBD, although the local orientation near the surface of the magnet was improved, the uneven diffusion caused by the squareness resulted in substantial deterioration (for example, the ratio of H_k to H_{c_j} decreased to a greater degree).

3.4 Magnetic field stability

Figure 6a shows the results of irreversible demagnetization experiments at higher temperatures for the CPMU18 made of PrFeB magnets (two $50\text{ mm} \times 30\text{ mm} \times 3.3\text{ mm}$ -sized magnets spliced with one $50\text{ mm} \times 30\text{ mm} \times 6.6\text{ mm}$ -sized magnet; orientation: 6.6 mm). As can be seen in the figure, the magnetic fields of the PrFeB magnets were stable at 25°C , and following the 75°C or 100°C treatments, the P42H and P48SH magnets displayed obvious irreversible demagnetization. The stability of the P48UH magnet was observed to be improved by 75°C or 100°C treatments. Figure 6b shows the magnetic field stability of the remaining P48SH magnets of the CPMU18 at a no-load state after 13 months (magnet size: $65\text{ mm} \times 25\text{ mm} \times 5.9\text{ mm}$; orientation: 5.9 mm). As detailed in the figure, after a long period in their natural

state, the P48SH magnets displayed different degrees of demagnetization. For example, the demagnetization rates of the 10 randomly selected magnets ranged between 1.25 and 2.15%. These results were determined to be closely related to such factors as the P48SH being characterized by large temperature coefficients, uneven microstructures, exposure to higher-temperature environments during the summer months, and so on.

4 The CPMU18 with PrFeB

The design index of the effective magnetic field peak value B_{eff} at 77 K for the first CPMU18 made of PrFeB magnets for SSRF was approximately 0.94 T at a gap of 6.0 mm. Table 2 shows the design parameters of the CPMU18 utilizing PrFeB magnets. It can be seen in the table that, if the P42H magnets were used as the magnetic field source, the effective magnetic field peak value could not reach the index, and the smaller H_{c_j} resulted in a poor resistance to demagnetization at room temperature. However, if the P48UH magnets were used as the magnetic field source, the CPMU18 could reach the designed 0.94 T at 77 K. In addition, the CPMU18 using P48UH magnets exhibited better demagnetization resistance. The magnetization angle of the magnets was observed to be poor, and at the same time, it had a relatively higher manufacturing cost. Therefore, further research and improvements are required to obtain an acceptable application level. The P48SH magnets displayed excellent comprehensive performance. The effective magnetic field peak value of the CPMU18 with P48SH magnets reached 0.96 T at 77 K, and the higher H_{c_j} resulted in a stronger anti-demagnetization resistance. Furthermore, the smaller magnetization angle caused the CPMU18 to have a good magnetic field quality.

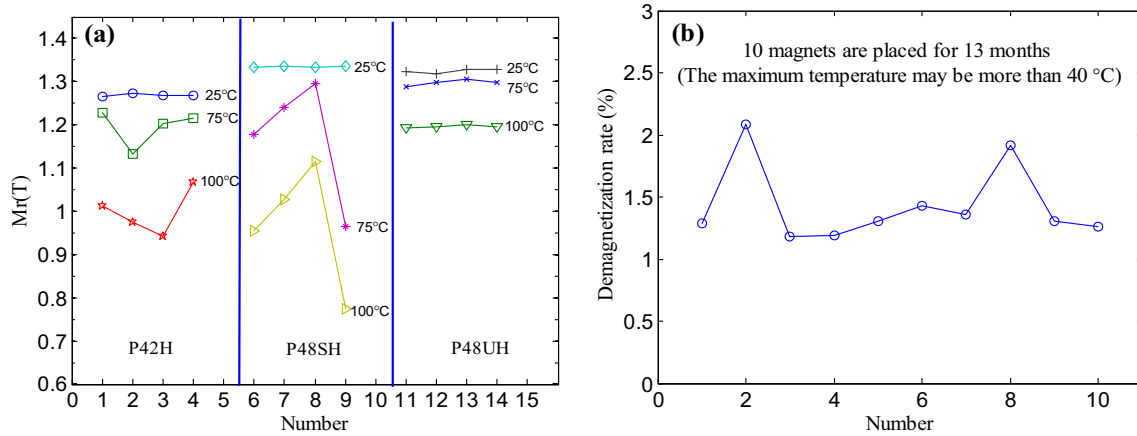


Fig. 6 (Color online) Irreversible demagnetization of PrFeB: **a** PrFeB magnets with CPMU magnetic circuit, **b** unloaded PrFeB magnet

Table 2 Magnet design parameters of CPMU18

Magnet/size	PrFeB/65.0 mm × 25.0 mm × 5.9 mm					
Pole/size	DT4C/43.0 mm × 20.0 mm × 3.0 mm					
Gap/L	6.0 mm/18.0 mm					
Grade	P42H		P48SH		P48UH	
T (K)	300	77	300	77	300	77
Br (T)	1.30	1.50	1.38	1.56	1.37	1.53
H _{cj} (kA/m)	1400	6000	1580	6000	2152	6000
B _{eff} (T)	0.82	0.93	0.85	0.96	0.85	0.94
H _d (kA/m)	1120	1265	1160	1320	1160	1300

Figure 7a shows the effective magnetic field peak values at the different gaps of the CPMU18 with P48SH magnets. It can be seen that the B_{eff} values were 0.82 T and 0.92 T at 300 K and 77 K, respectively, when the gap was 6 mm. However, there was still a difference observed from the designed effective magnetic field. The main reasons for this problem were as follows: ① The finite element calculation

accuracy of the magnetic field for the CPMU was approximately 1%, and a certain amount of error occurred between the measured and calculated values. ② The effective peak magnetic field is closely related to the magnetic gap of the CPMU18, and there may be some error in the calculation of the gap of the CPMU18. ③ The decreases in cycle length experienced by the CPMU18 at low temperatures caused some loss of the magnetic field. ④ The unstable characteristics of the PrFeB magnets themselves caused large, irreversible magnetic field losses. The comprehensive analyses of similar CPMU research results from international research groups along with the experimentally obtained demagnetization data of the P48SH magnets are shown in Fig. 6b. It was determined that the irreversible demagnetization caused by the environmental temperatures experienced by the P48SH magnets for the CPMU18 was the main reason for the failure of the CPMU18 magnetic field to reach the design index. The contribution ratios of the magnetic field calculation, gap measurement error, and decreases in CPMU period length

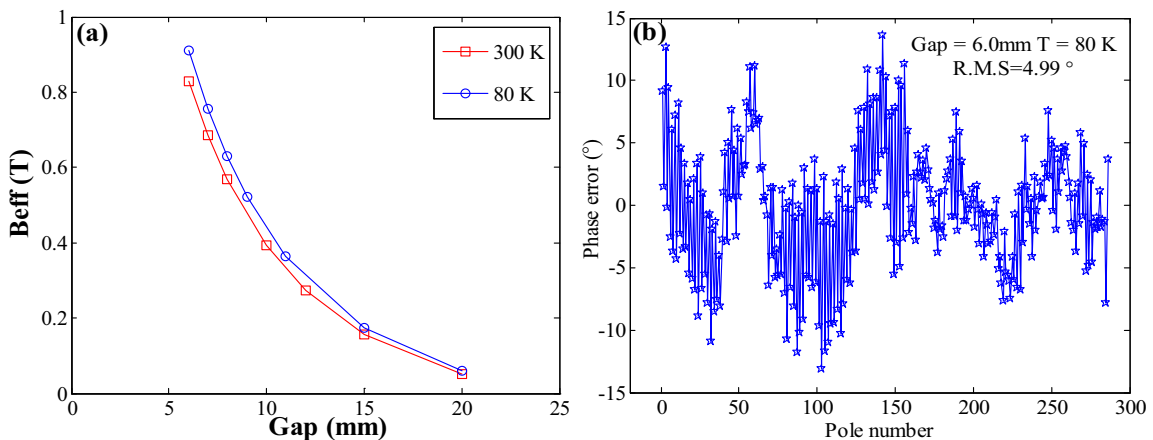


Fig. 7 (Color online) **a** Effective peak magnetic field of CPMU18 and **b** magnetic field phase error of CPMU18

to the magnetic field losses remain areas for further study and analysis in the future.

Figure 7b shows the magnetic field phase error of CPMU18 with P48SH magnets when gap was 6.0 mm and the temperature was 80 K. It can be seen that the RMS phase error of CPMU18 was about 4.99°.

5 Conclusion

The $(BH)_{\max} + H_k$ values of the three kinds of PrFeB magnets (P42H, P48SH, and P48UH) were 57.4, 65.3, and 66.1, respectively. Compared with $\text{Sm}_2\text{Co}_{17}$ and NdFeB, PrFeB magnets can achieve greatly increased Br and H_{cj} values at low temperature. Through the optimization of the preparation method and composition design, the orientation degree of the P42H, P48UH, and P48SH magnets gradually improved, while the P48UH magnet exhibited a decreased H_k/H_{cj} ratio due to the uneven distribution of Tb. The magnetic field uniformity of the P48SH magnets was found to be good, but the magnetization angles of the P42H and P48UH magnets remain to be further improved. With the increase in H_{cj}, the magnetic field stability of the P42H, P48SH, and P48UH magnets gradually improved; in particular, P48UH was found to withstand high-temperature baking of the CPMU. The three kinds of PrFeB magnets prepared in this work have application value in the field of synchrotron radiation, free electron lasers, and space instruments. For P42H magnets, the H_{cj} is lower and the magnetization angle is too large, so the magnetic circuit design should fully consider demagnetization, uniformity of magnetic field, and other factors. If P48UH can solve the problem of its magnetization angle, it is expected to be more important for practical applications. The comprehensive performance of P48SH magnets was found to be excellent. Using the PrFeB permanent magnet as magnetic field source, the first cryogenic permanent magnet undulator CPMU18 of China has been developed; when the temperature was 80 K and the gap was 6.0 mm, the magnetic field measurement results showed that the effective the peak field was 11.76% higher than at 300 K, reaching 0.92 T, with an RMS phase error of about 4.99°.

References

1. H. Onuki, *Wigglers, Undulators and Their Applications* (Taylor & Francis, London, 2003), pp. 176–255
2. Z.H. Mai, *Synchrotron Light Source and Its Applications* (Science Press, Beijing, 2013), pp. 35–38
3. S.M. Yang, C. Feng, D.Z. Huang et al., Wakefields studies for the SXFEL user facility. *Nucl. Sci. Tech.* **28**(7), 90 (2017). <https://doi.org/10.1007/s41365-017-0242-7>
4. S.Z. Zhou, *Sintered NdFeB Rare Earth Permanent Magnet Materials and Technology* (Metallurgical Industry Press, Beijing, 2011), pp. 1–13
5. Y.Z. He, Q.G. Zhou, Application of magnetic materials in synchrotron radiation and free electron laser. *J. Inorg. Mater.* **31**(10), 1021 (2016). <https://doi.org/10.15541/jim20160177>
6. Y.Z. He, The research on magnetic properties of permanent magnet and magnetic field of prototype for cryogenic permanent magnet undulator, Ph.D. Dissertation, Chinese Academy of Sciences University, Beijing, 2015. CNKI:CDMD:1.1015.033040
7. C. Benabderrahmane, N. Béchu, P. Berteaud et al., Development of a PrFeB cryogenic undulator at SOLEIL, in *Proceedings of IPAC'10, Kyoto*, WEPD007, (2010), p. 3096
8. J. Bahrtdt, H.-J. Bäcker, M. Dirsatt et al., Cryogenic design of a PrFeB-based undulator, in *Proceedings of IPAC'10, Kyoto*, WEPD012 (2010), p. 3111
9. J. Bahrtdt, W. Frentrop, A. Gauppa et al., Cryogenic undulator for a table top FEL. *AIP Conf. Proc.* **1234**, 499 (2010). <https://doi.org/10.1063/1.3463250>
10. Q. Zhou, Grain boundary structure and grain boundary phase modifications and their effects on properties of sintered NdFeB permanent magnets, Ph.D. Dissertation, South China university of Technology National, Guangzhou, 2016
11. K. Hirota, H. Nakamura, T. Minowa et al., Coercivity enhancement by the grain boundary diffusion process to Nd–Fe–B sintered magnets. *IEEE Trans. Magn.* **42**(10), 2909 (2006). <https://doi.org/10.1109/tmag.2006.879906>
12. Y.Z. He, X.Q. Bao, Q.G. Zhou et al., Magnetic field stability of PrFeB magnets developed by GBD for cryogenic permanent magnet undulators. *J. Rare Earths* **36**, 385–389 (2018). <https://doi.org/10.1016/j.jre.2017.09.011>
13. D.X. Chen, E. Pardo, Y.H. Zhu, Demagnetizing correction in fluxmetric measurements of magnetization curves and hysteresis loops of ferromagnetic cylinders. *J. Magn. Magn. Mater.* **449**, 447–454 (2018). <https://doi.org/10.1016/j.jmmm.2017.10.069>
14. Y.Z. He, Inhomogeneity of external magnetic field for permanent magnet. *Acta Phys. Sin.* **62**(8), 084105 (2013). <https://doi.org/10.7498/aps.62.084105>